Three-body forces and neutron star structure

X. R. Zhou,[1,2] G. F. Burgio,[3] U. Lombardo,[2] H.-J. Schulze,[3] and W. Zuo[4]
[1]*Department of Physics, Tsinghua University, 100084 Beijing, China*
[2]*INFN-LNS, Via Santa Sofia 44, I-95123 Catania, Italy*
[3]*INFN Sezione di Catania, Via Santa Sofia 64, I-95123 Catania, Italy*
[4]*Institute of Modern Physics, 730000 Lanzhou, China*
(Received 16 July 2003; published 5 January 2004)

We calculate the nucleonic equation of state within the Brueckner-Bethe-Goldstone formalism using the Argonne v_{18} two-body interaction and a three-body interaction. We adopt two different three-body forces: the phenomenological Urbana IX model and a microscopic meson-exchange force including nucleon virtual excitations and nucleon-antinucleon excitations. We compare their respective predictions regarding the structure of neutron stars, in particular the mass-radius relation.

DOI: 10.1103/PhysRevC.69.018801 PACS number(s): 21.65.+f, 26.60.+c, 24.10.Cn, 97.60.Jd

The theoretical description of neutron stars requires the knowledge of the nuclear matter equation of state (EOS) at very high densities, reaching about ten times the saturation density of nuclear matter, $n_0 \approx 0.17$ fm^{-3}. The results are therefore very sensitive to the theoretical modeling of high density nuclear matter.

In this Brief Report we investigate this sensitivity within the microscopic Brueckner-Bethe-Goldstone description of nuclear matter [1]. The basic ingredient is the Brueckner reaction matrix G, which is the solution of the Bethe-Goldstone equation,

$$G[\omega;n] = V + \sum_{k_a k_b} V \frac{|k_a k_b\rangle Q \langle k_a k_b|}{\omega - e(k_a) - e(k_b) + i\epsilon} G[\omega;n], \quad (1)$$

where V is the bare nucleon-nucleon (NN) interaction, n is the nucleon number density, and ω the starting energy. The single-particle energy $e(k)$ (assuming $\hbar = 1$),

$$e(k) = e(k;n) = \frac{k^2}{2m} + U(k;n), \quad (2)$$

and the Pauli operator Q constrain the propagation of intermediate baryon pairs above the Fermi momentum. The Brueckner-Hartree-Fock (BHF) approximation for the single-particle potential $U(k;n)$ using the *continuous choice* prescription is

$$U(k;n) = \mathrm{Re} \sum_{k' \le k_F} \langle kk'|G[e(k) + e(k');n]|kk'\rangle_a, \quad (3)$$

where the subscript a indicates antisymmetrization of the matrix elements. Because of the occurrence of $U(k;n)$ in Eq. (2), Eqs. (1)–(3) constitute a coupled system of equations that needs to be solved self-consistently for different Fermi momenta. In the BHF approximation the energy per nucleon is given by

$$\frac{E}{A} = \frac{3}{5}\frac{k_F^2}{2m} + \frac{1}{2n} \mathrm{Re} \sum_{k,k' \le k_F} \langle kk'|G[e(k) + e(k');n]|kk'\rangle_a. \quad (4)$$

The basic input quantity in the Bethe-Goldstone equation (1) is the nucleon-nucleon (NN) interaction in free space, V. In this work we adopt the new Argonne v_{18} potential [2] as a model for the free two-nucleon interaction.

It is well known that the standard BHF formalism involving only two-body forces does not reproduce correctly the empirical saturation point of nuclear matter, despite its rapid convergence when including three-hole line contributions [3]. This drawback is usually overcome by including three-body forces (TBF). Two major lines of this approach have been pursued in the past, one involving a semiphenomenological determination of the TBF [4–6], the other a completely microscopic model based on meson exchange with intermediate excitation of nucleon resonances [7–9]. Since the phenomenological TBF are also widely used in variational [10,11] and quantum Monte Carlo [12–14] calculations of nuclear matter, it is clearly of interest to compare the two approaches. This is the purpose of the present paper, which is actually focused on astrophysical applications, namely, the prediction of neutron star structure based on a nucleonic BHF equation of state employing the various TBF.

We begin with a short overview of the theoretical formalism concerning the phenomenological Urbana IX TBF [4–6,12]. For the description of the microscopic approach, the reader is referred to Refs. [7–9], where TBF are discussed in great detail. We remind that the Urbana IX TBF model contains a two-pion exchange potential $V_{ijk}^{2\pi}$ supplemented by a phenomenological repulsive term V_{ijk}^{R},

$$V_{ijk} = V_{ijk}^{2\pi} + V_{ijk}^{R}, \quad (5)$$

where

$$V_{ijk}^{2\pi} = A \sum_{\mathrm{cyc}} \Big[\{X_{ij}, X_{jk}\}\{\boldsymbol{\tau}_i \cdot \boldsymbol{\tau}_j, \boldsymbol{\tau}_j \cdot \boldsymbol{\tau}_k\} + \frac{1}{4}[X_{ij}, X_{jk}][\boldsymbol{\tau}_i \cdot \boldsymbol{\tau}_j, \boldsymbol{\tau}_j \cdot \boldsymbol{\tau}_k] \Big], \quad (6)$$

$$V_{ijk}^{R} = U \sum_{\text{cyc}} T^2(m_\pi r_{ij}) T^2(m_\pi r_{jk}). \quad (7)$$

The two-pion exchange operator X_{ij} is given by

$$X_{ij} = Y(m_\pi r_{ij}) \boldsymbol{\sigma}_i \cdot \boldsymbol{\sigma}_j + T(m_\pi r_{ij}) S_{ij}, \quad (8)$$

where $\boldsymbol{\sigma}$ and $\boldsymbol{\tau}$ are the Pauli spin and isospin operators, and $S_{ij} = 3(\boldsymbol{\sigma}_i \cdot \hat{\mathbf{r}}_{ij})(\boldsymbol{\sigma}_j \cdot \hat{\mathbf{r}}_{ij}) - \boldsymbol{\sigma}_i \boldsymbol{\sigma}_j$ is the tensor operator. Y and T are the Yukawa and tensor functions, respectively, associated to the one-pion exchange:

$$Y(x) = \frac{e^{-x}}{x}(1 - e^{-cr^2}), \quad (9)$$

$$T(x) = \left(1 + \frac{3}{x} + \frac{3}{x^2}\right) \frac{e^{-x}}{x} (1 - e^{-cr^2})^2. \quad (10)$$

For the use in BHF calculations, this TBF is reduced to an effective, density dependent, two-body force by averaging over the third nucleon in the medium, taking account of the nucleon-nucleon correlations by means of the BHF defect function g,

$$\bar{V}(\mathbf{r}_{ij}) = n \int d^3 r_k \sum_{\sigma_k, \tau_k} V_{ijk} [1 - g(r_{ik})]^2 [1 - g(r_{jk})]^2. \quad (11)$$

This procedure yields an effective two-nucleon potential of a simple structure,

$$\bar{V}(\mathbf{r}) = \boldsymbol{\tau}_i \cdot \boldsymbol{\tau}_j [\boldsymbol{\sigma}_i \cdot \boldsymbol{\sigma}_j V_C^{2\pi}(r) + S_{ij}(\hat{\mathbf{r}}) V_T^{2\pi}(r)] + V^R(r), \quad (12)$$

containing central and tensor two-pion exchange components as well as a central repulsive contribution.

The two parameters A and U are usually determined by either, in the variational approach, fitting the triton binding energy together with the saturation density of nuclear matter (yielding however too little attraction, $B/A \approx -12$ MeV, in the latter case [10]), or, in the BHF calculations, reproducing the empirical saturation density together with the binding energy of nuclear matter. The resulting parameter values are $A = -0.0293$ MeV and $U = 0.0048$ MeV (as well as $c = 2.1$ fm^{-2}) in the variational Urbana IX model, whereas for the optimal BHF+TBF calculations (yielding a saturation point at $k_F \approx 1.36$ fm^{-1}, $B/A \approx -15.5$ MeV, and an incompressibility $K \approx 210$ MeV) we require $A = -0.0333$ MeV and $U = 0.00038$ MeV. These values of A and U have been obtained by using the Argonne v_{18} two-body force both in the BHF and in the variational many-body theories. However, the required repulsive component is much weaker in the BHF approach, consistent with the observation that in the variational calculations usually heavier nuclei as well as nuclear matter are underbound. Indeed, less repulsive TBF became available recently [14] in order to address this problem.

We now turn to the discussion of our numerical results. In Fig. 1 we display for symmetric matter (upper panel) and pure neutron matter (lower panel) the BHF defect function g as a function of the interparticle distance r at several densities. To be more precise, we actually plot the defect function averaged over the $^1S_0$ and $^3SD_1$ partial waves (only $^1S_0$ for neutron matter), with one momentum being k_F and the other averaged over the Fermi sphere. One notes that the dependence on density (as well as that on the two momenta) is actually rather weak, allowing eventually to keep the defect function fixed for calculations at different densities. In this case the averaged TBF potential, Eq. (11), would depend purely linear on density.

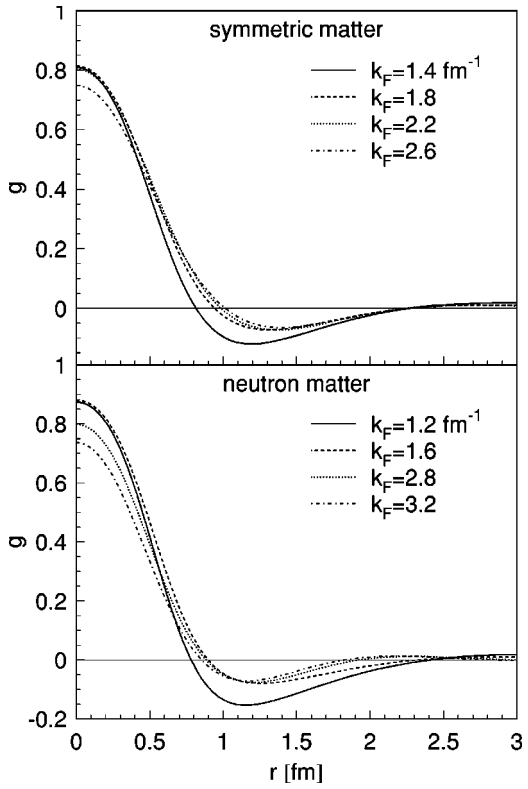

FIG. 1. BHF defect functions in symmetric nuclear matter and neutron matter at different densities.

In Fig. 2 we show the different components $V_C^{2\pi}$, $V_T^{2\pi}$, and V^R [Eq. (12)] of the averaged TBF potential in symmetric matter at normal density. Comparing to the microscopic TBF of Ref. [8], one can roughly identify $V^{2\pi}$ with the combined effect of π and ρ meson exchanges (cf. Fig. 10 in Ref. [8]), whereas V^R simulates the interaction due to the various σ, ω exchanges (Fig. 11 of the same reference). With the choice of parameters A and U given above, the different phenomenological potentials are of similar shape and magnitude as the corresponding microscopic results.

The resulting binding energy per nucleon for symmetric nuclear matter and purely neutron matter is shown in Fig. 3. In this figure we compare results obtained within the BHF approach without TBF (dotted curve), with the microscopic TBF (solid curve), and with the phenomenological ones constructed with the choice of parameters given above. In the latter case, we compare for completeness calculations using the G matrix (dot-dashed curve) and the K matrix (dashed curve), i.e., neglecting the imaginary part of the G matrix in Eq. (1). We notice that up to a density of $n \approx 0.4$ fm^{-3} the results using microscopic and phenomenological TBF are in fair agreement, whereas at higher density the microscopic TBF turn out to be more repulsive. For convenience, we

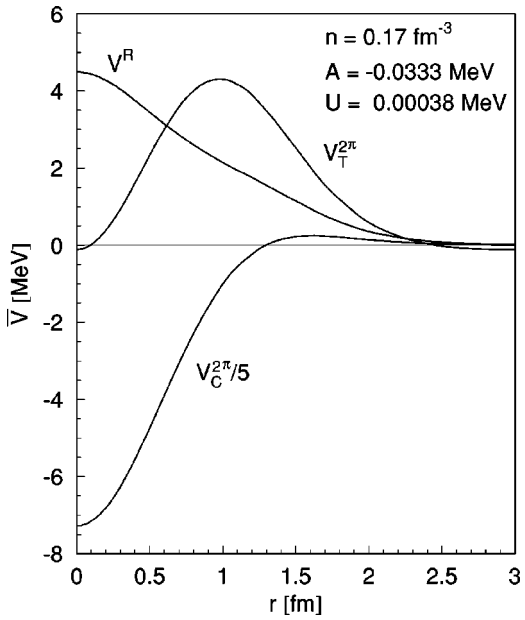

FIG. 2. Averaged BHF TBF potentials, Eq. (12), calculated for symmetric matter at normal density.

provide empirical parametrizations of our numerical results of the functional form

$$\frac{B}{A}(n) = \alpha n + \beta n^{\gamma}. \tag{13}$$

The parameters α, β, γ are listed in Table I for the different EOS.

In order to study the effects of different TBF on neutron star structure, we have to calculate the composition and the equation of state of cold, catalyzed matter. We require that the neutron star contains charge neutral matter consisting of neutrons, protons, and leptons in β equilibrium. No transitions to other phases are considered in this paper. Following standard procedures [15], we compute the proton fraction and the equation of state for charge neutral and β-stable matter, using the various TBF discussed above.

TABLE I. Parameters of the EOS fit, Eq. (13), for symmetric nuclear matter (SNM) and pure neutron matter (PNM) using different TBF.

	α	β	γ
SNM, micro	−178.2	435.2	2.00
SNM, pheno(G)	−290.7	397.7	1.38
SNM, pheno(K)	−265.5	406.0	1.47
PNM, micro	91.5	471.9	3.00
PNM, pheno(G)	83.3	237.2	2.34
PNM, pheno(K)	77.1	257.4	2.27

In Fig. 4 we display the symmetry energy and the proton fraction as functions of the nucleon density n for different choices of the TBF. We observe results in agreement with the characteristics of the EOS shown in Fig. 3. In fact, the stiffest equation of state, i.e., the one calculated with the microscopic TBF, yields larger symmetry energies compared to the ones obtained with the phenomenological TBF. As a consequence, the proton fraction is correspondingly larger.

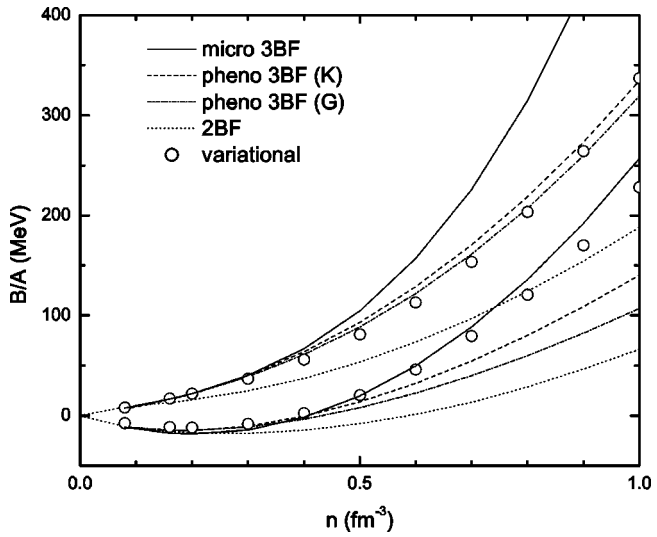

FIG. 3. Binding energy per nucleon of symmetric nuclear matter (lower curves using a given linestyle) and pure neutron matter (upper curves), employing different TBF. See text for details.

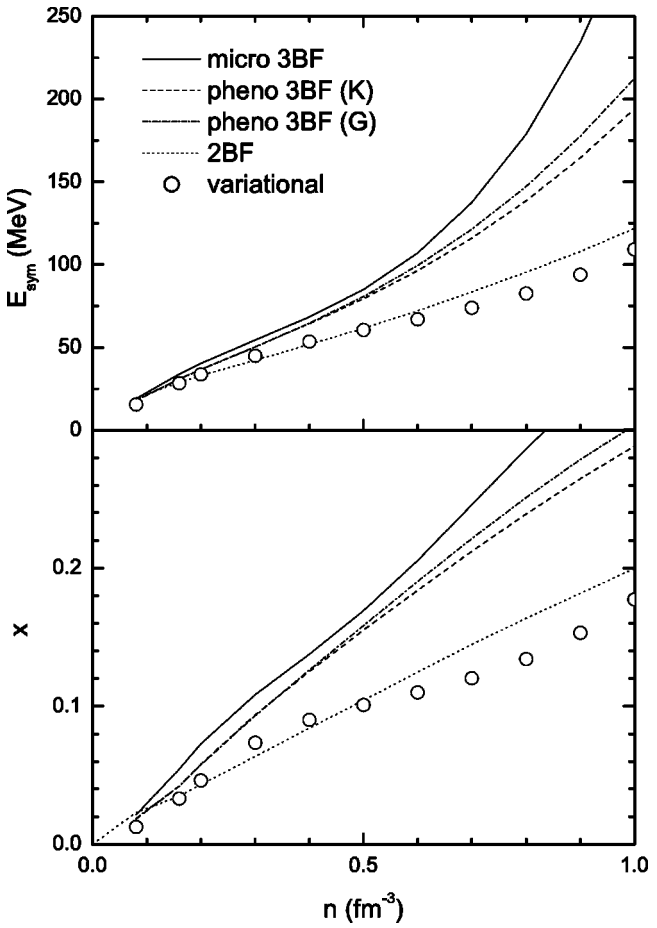

FIG. 4. Symmetry energy (upper panel) and proton fraction (lower panel) of β-stable matter using different TBF.

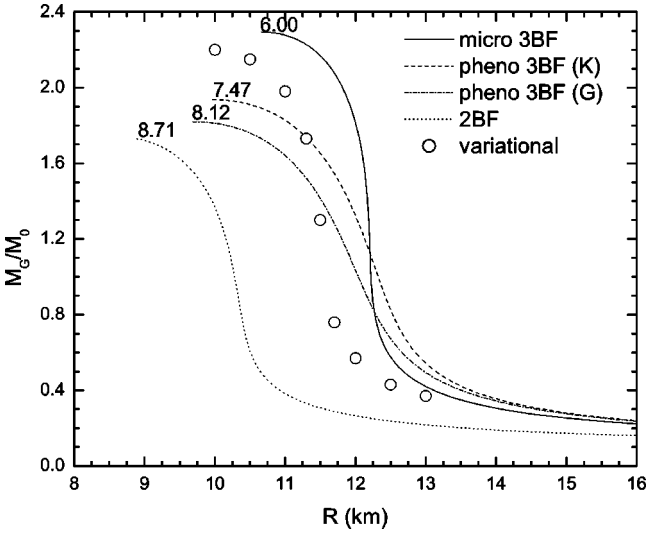

FIG. 5. Mass-radius relations of neutron stars evaluated with different equations of state. The numbers near the curves denote the central density n_c/n_0 of the maximum mass configuration.

In order to calculate the mass-radius relation, one has to solve the well-known Tolman-Oppenheimer-Volkov equations [15], with the newly constructed EOS for the charge neutral and β-stable case as input. The results are shown in Fig. 5. We notice that the EOS calculated with the microscopic TBF produces the largest gravitational masses, with the maximum mass of the order of 2.3 $M_\odot$, whereas the phenomenological TBF yields a maximum mass of about 1.9 $M_\odot$. In the latter case, neutron stars are characterized by smaller radii and larger central densities, i.e., the Urbana TBF produce more compact stellar objects.

For completeness, we also compare our results shown in Figs. 3–5 with the ones obtained by Akmal *et al.* [10] within the variational method, using the same Argonne v_{18} two-body potential and the Urbana IX model (the repulsive term V^R reduced by 37%, however) as three-nucleon interaction. It can be seen that this calculation predicts smaller symmetry energies, close to the BHF values without TBF, as well as maximum masses in the same range as those of the BHF +TBF models. The discrepancies are due to the different many-body approaches.

However, in the end it should be emphasized that our results overestimate the effect of the differences between the nucleonic TBF. In reality, in particular the early appearance of hyperons [16] (as well as eventually quark matter [17]) at densities of about $n \approx (2, \ldots, 3)n_0$ renders the effect of the nucleonic TBF much less important, because the nucleonic partial densities inside the star remain more limited. (In Ref. [16] a reduction of the maximum central *nucleonic* density by about 40% was reported, for example).

In conclusion, it seems justified to use the phenomenological Urbana IX TBF in situations where the nucleonic EOS is probed up to densities $n \approx (3, \ldots, 4)n_0$. However, as noted before, in order to reproduce the correct saturation point of nuclear matter, as well as to be compatible with the microscopic TBF, the repulsive component V^R in the BHF approach has to be chosen an order of magnitude smaller than in the variational calculations.

We would like to acknowledge valuable discussions with M. Baldo.

[1] M. Baldo, *Nuclear Methods and the Nuclear Equation of State* (World Scientific, Singapore, 1999).
[2] R. B. Wiringa, V. G. J. Stoks, and R. Schiavilla, Phys. Rev. C **51**, 38 (1995).
[3] H. Q. Song, M. Baldo, G. Giansiracusa, and U. Lombardo, Phys. Rev. Lett. **81**, 1584 (1998); M. Baldo, A. Fiasconaro, H. Q. Song, G. Giansiracusa, and U. Lombardo, Phys. Rev. C **65**, 017303 (2002).
[4] B. S. Pudliner, V. R. Pandharipande, J. Carlson, and R. B. Wiringa, Phys. Rev. Lett. **74**, 4396 (1995).
[5] M. Baldo, I. Bombaci, and G. F. Burgio, Astron. Astrophys. **328**, 274 (1997).
[6] M. Baldo and L. S. Ferreira, Phys. Rev. C **59**, 682 (1999).
[7] S. A. Coon, M. D. Scadron, P. C. McNamee, B. R. Barrett, D. W. E. Blatt, and B. H. J. McKellar, Nucl. Phys. **A317**, 242 (1979).
[8] P. Grangé, A. Lejeune, M. Martzolff, and J.-F. Mathiot, Phys. Rev. C **40**, 1040 (1989).
[9] A. Lejeune, U. Lombardo, and W. Zuo, Phys. Lett. B **477**, 45 (2000); W. Zuo, A. Lejeune, U. Lombardo, and J.-F. Mathiot, Eur. Phys. J. A **14**, 469 (2002); Nucl. Phys. **A706**, 418 (2002).
[10] A. Akmal, V. R. Pandharipande, and D. G. Ravenhall, Phys. Rev. C **58**, 1804 (1998).
[11] J. Morales, V. R. Pandharipande, and D. G. Ravenhall, Phys. Rev. C **66**, 054308 (2002).
[12] B. S. Pudliner, V. R. Pandharipande, J. Carlson, S. C. Pieper, and R. B. Wiringa, Phys. Rev. C **56**, 1720 (1997).
[13] R. B. Wiringa, S. C. Pieper, J. Carlson, and V. R. Pandharipande, Phys. Rev. C **62**, 014001 (2000).
[14] S. C. Pieper, V. R. Pandharipande, R. B. Wiringa, and J. Carlson, Phys. Rev. C **64**, 014001 (2001).
[15] S. Shapiro and S. A. Teukolsky, *Black Holes, White Dwarfs, and Neutron Stars* (Wiley, New York, 1983).
[16] M. Baldo, G. F. Burgio, and H.-J. Schulze, Phys. Rev. C **58**, 3688 (1998); **61**, 055801 (2000).
[17] G. F. Burgio, M. Baldo, P. K. Sahu, and H.-J. Schulze, Phys. Rev. C **66**, 025802 (2002); M. Baldo, M. Buballa, G. F. Burgio, F. Neumann, M. Oertel, and H.-J. Schulze, Phys. Lett. B **562**, 153 (2003).